World Journal of Advanced Research and Reviews
eISSN: 2581-9615 CODEN (USA): WJARAI
Cross Ref DOI: 10.30574/wjarr
Journal homepage: https://wjarr.com/

(RESEARCH ARTICLE)

Check for updates

Contribution of X-ray diffraction (XRD) to the identification of mineral phases in the gold systems of the Kouroussa Gold Mine site, Republic of Guinea

Aboubacar SOUMAH [1, 2, *], Gnammytchet Barthélémy KOFFI [2], Mory KOUROUMA [1], Gianluigi ROSATELLI [3], Amedeo CINOSI [4] and Mohamed Lamine SYLLA [1]

[1] *Institute Supérieur des Mines et Géologie de Boké (ISMGB), B.P. 84, Boké, République de Guinée.*
[2] *Institute National Polytechnique Felix Houphouët-Boigny (INP–HB), B.P. 1093, Yamoussoukro, Côte d'Ivoire*
[3] *Università degli Studi "G. d'Annunzio" Chieti – Pescara, Dipartimento di Scienze, Via dei Vestini, 3166100 Chieti, Italy.*
[4] *Analytical Instruments Group, Via Torino, 7-28010 Agrate Conturbia (NO), Italy.*

World Journal of Advanced Research and Reviews, 2026, 30(02), 1684-1694

Publication history: Received on 08 April 2026; revised on 13 May 2026; accepted on 16 May 2026

Article DOI: https://doi.org/10.30574/wjarr.2026.30.2.1371

Abstract

This study evaluates the contribution of X-ray diffraction (XRD) to the identification and quantification of mineral phases within the gold-bearing systems of the Kouroussa permit, located in the Birimian domain of the West African Craton. Seventy samples collected from outcrops and drill cores from eight boreholes (>1400 m) were investigated, among which ten representative samples were selected for detailed analyses. After fine grinding to 75 µm, particle-size reduction and addition of a calcined ZnO internal standard (5 wt.%), analyses were performed using XRD diffractometry (Bruker D2 Phaser, 5–80° 2θ). Mineral phases were identified using DIFFRAC.EVA software and quantified through Rietveld refinement with PROFEX 5.The results reveal strong variability in mineral assemblages. Quartz dominates highly silicified zones, reaching 49 wt.% (C036) and 69 wt.% (C050). Feldspars and plagioclases characterize magmatic lithologies with cumulative contents up to 73 wt.% (C009). Carbonates, particularly abundant in sample C014 (48 wt.%), indicate carbonation related to CO_2-rich fluids. Ferromagnesian minerals, mainly chlorite and biotite, reflect greenschist-facies hydrothermal alteration. Sulfides, especially pyrite and arsenopyrite, are concentrated within mineralized zones, with local occurrences of native gold.The interpretation highlights three successive evolutionary stages: an initial magmatic phase, a hydrothermal phase marked by silicification, chloritization and carbonation, followed by a sulfide-gold mineralization stage. The most prospective mineralized zones are associated with intense silicification, strong hydrothermal alteration and high sulfide concentrations, confirming the effectiveness of XRD as a mineralogical vectoring tool in Birimian gold systems of Kouroussa.

Keywords: XRD; Mineralogy; Gold system; Birimian; Kouroussa

1. Introduction

Understanding gold-bearing systems largely relies on the identification of mineral phases and paragenetic associations, which are key indicators of the geological and hydrothermal processes responsible for gold deposit formation [1,2]. In the Birimian formations of West Africa, gold mineralization is commonly associated with tectono-metamorphic events and hydrothermal fluid circulations linked to sulfides such as pyrite, arsenopyrite, chalcopyrite, sphalerite, and galena [3–9]. The study of these mineral assemblages is essential for improving the understanding of metallogenic processes and optimizing mineral exploration strategies.

Among the analytical methods used in mineralogical characterization, X-ray diffraction (XRD) is a reliable technique for identifying crystalline phases in complex and polyphased materials [10–17]. It provides valuable information on the

* Corresponding author: Aboubacar SOUMAH

mineralogical composition of rocks and helps identify minerals related to hydrothermal alteration and mineralization processes. However, this method also presents limitations, particularly in detecting amorphous phases or minerals occurring in very low proportions [10,16,18,19].

The Kouroussa Gold Mining (KGM) permit, located within the Birimian geological context of Guinea, represents a favorable setting for the study of hydrothermal gold systems [5,20,21]. Despite its economic importance, detailed data on mineral associations and gold-bearing phases remain limited. In this context, the present study aims to evaluate the contribution of XRD to the identification of mineral phases within the gold-bearing systems of the Kouroussa permit, in order to characterize mineral assemblages and discuss their metallogenic implications.

1.1. Presentation and geological context

The study area is located in eastern Guinea, West Africa, at latitude 10°43' N and longitude 9°52' W. The project site is situated approximately 3 km from the town of Kouroussa and about 570 km east of Conakry, the capital city of the Republic of Guinea, accessible by paved road (Figure 1). Kouroussa is a prefecture in Guinea, located in Haute-Guinée (Upper Guinea) within the Kankan region. It sits at an altitude of 362 meters and is watered by the Niger River. The prefecture covers 14,050 km^2 and is divided into 14 sub-prefectures. It is home to 451,205 inhabitants according to the RGPH-4 census of 2025, of whom 69,215 live in the urban area of Kouroussa-Centre.

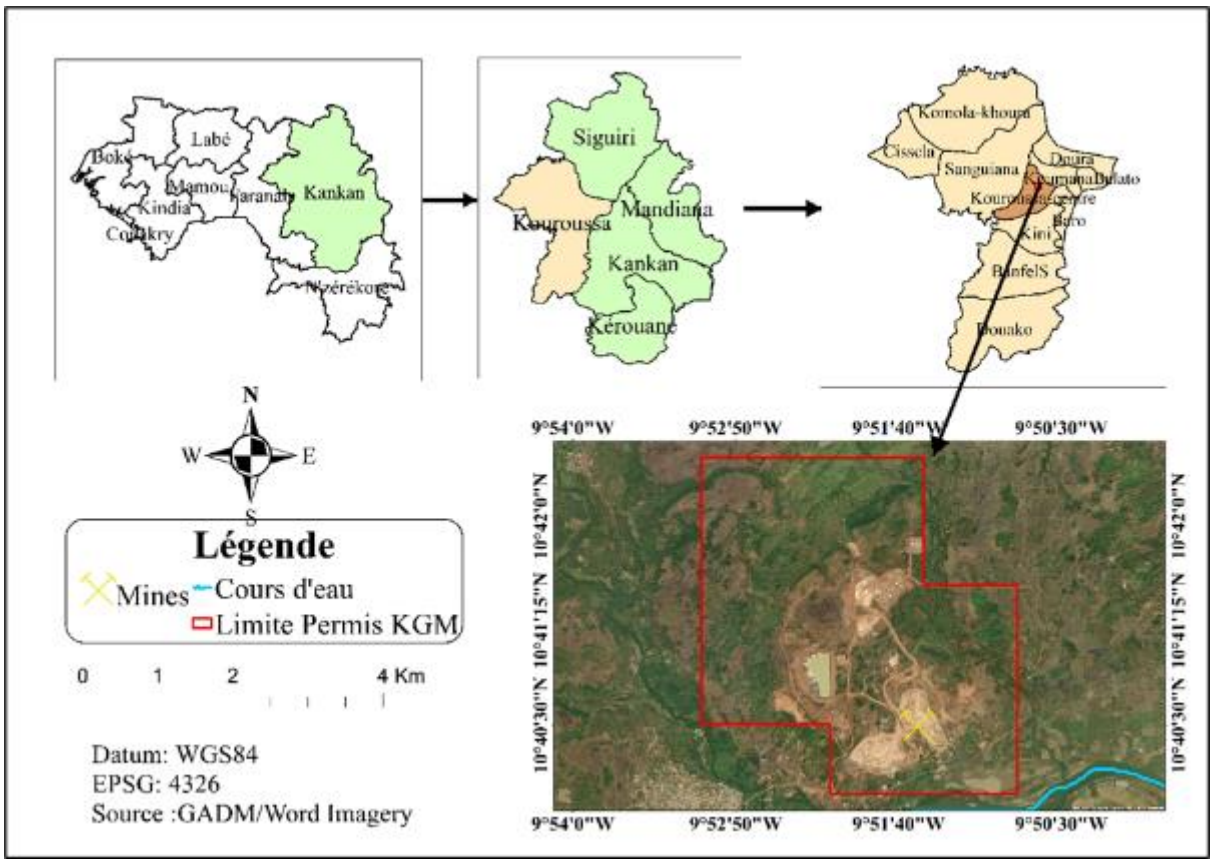

Figure 1 Presentation of the study area

The Kouroussa gold project is located within the Paleoproterozoic Siguiri Basin, which belongs to the Birimian volcano-sedimentary system of the West African Craton, host to numerous major gold deposits. The basement consists of the Archean Man Shield, composed of high-grade metamorphic rocks and granitoid intrusions. It is separated from the Birimian units by the Nandian Belt, associated with early volcanic episodes related to rifting processes.

The Eburnean orogeny led to the development of NE–SW to NW–SE deformation zones and granitoid intrusions. These structures, together with greenschist-facies metamorphism, strongly control gold mineralization within the Siguiri Basin.

The Kouroussa area is largely covered by intensely weathered lateritic plateaus, with colluvial and alluvial deposits. This cover commonly masks the bedrock, making drilling data essential for geological interpretation. The basement is dominated by Birimian volcano-sedimentary sequences composed of mudstones, siltstones, feldspathic sandstones, and carbonate layers, associated with mafic to ultramafic volcanic units and cherts. The overall structural trend is predominantly north-northwest (source: KGM internal data).

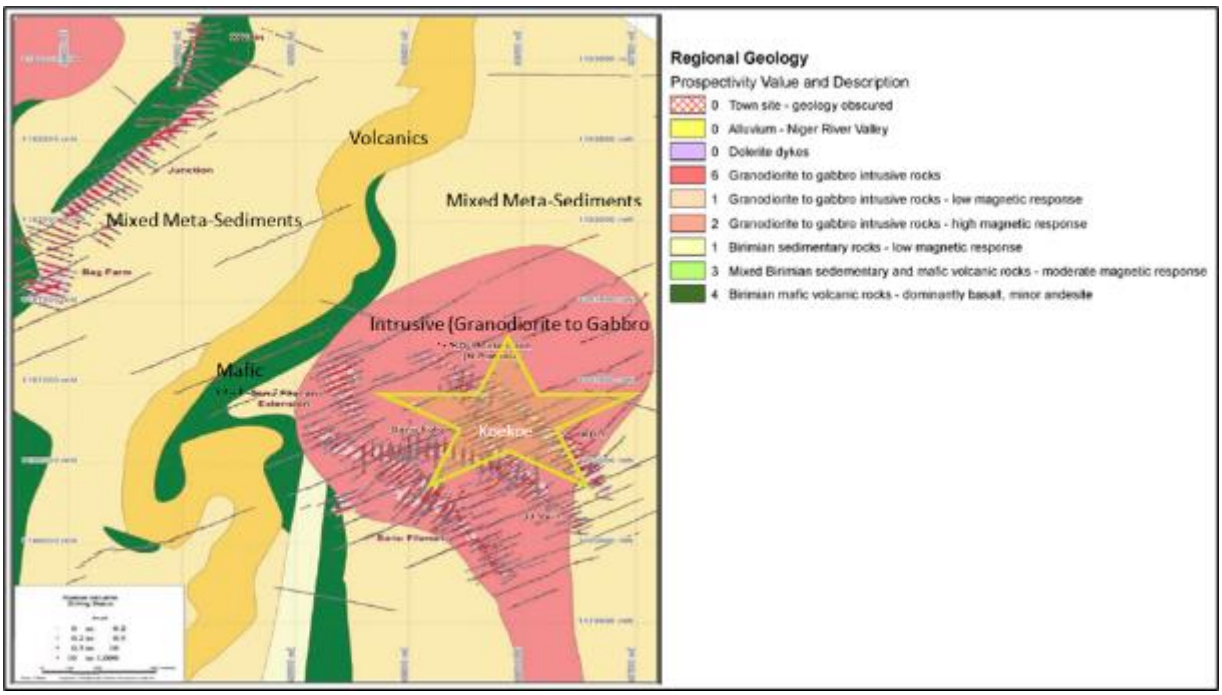

Figure 2 Geological map of the Kouroussa permit (KGM, 2024)

Figure 2 presents the geological map of the Kouroussa permit (source: KGM internal data). It shows the distribution of the main lithological units and major tectonic structures. The area is dominated by Birimian sequences intruded by granitoids and locally associated with mafic to ultramafic volcanic rocks. NNW-oriented shear zones constitute the principal pathways for hydrothermal fluid circulation and strongly control the localization of gold mineralization.

2. Materials and Methods

Field investigations were carried out in August and September 2024. The work included geological mapping, lithological and structural descriptions, and sampling conducted on outcrops and drill cores from eight (8) boreholes, representing a cumulative length of more than 1400 m. A total of 70 samples were collected, covering the main lithological units of the area, including magmatic intrusions, metasedimentary rocks, quartz veins (oxidized and smoky), and saprolites. Macroscopic observations of the drill cores were performed using a hand lens (10×20 mm), allowing the description of textures, alteration features, and structures associated with gold mineralization. Ten (10) representative samples were selected for this study (Figure 3).

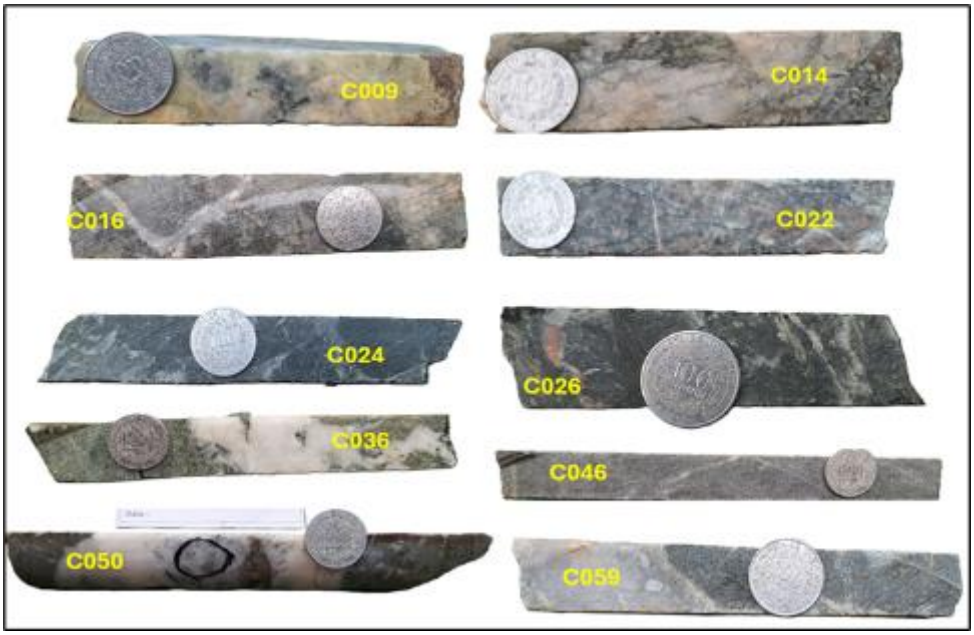

Figure 3 Macroscopic photographs of rock samples (C009, C014, C016, C022, C024, C026, C036, C046, C050, and C059) illustrating textures, structures, and hydrothermal alteration associated with the Kouroussa gold systems

The studied samples mainly display lithological types associated with quartz veins, which are typical of the hydrothermal gold systems of Kouroussa. Sample C009 is light-colored, massive, and strongly silicified, with oxidation traces indicating sulfide alteration. Sample C014 exhibits a slightly foliated texture with deformed quartz veins, reflecting tectonic deformation and fluid circulation. Samples C016 and C059 show marked foliation and a greenish coloration related to chloritization, indicating moderate hydrothermal alteration, whereas C022 remains relatively homogeneous with a few quartz-filled fractures.

The dark-colored samples C024 and C026 are massive and probably mafic, containing quartz veinlets; C026 additionally displays oxidized zones suggesting the presence of sulfides. Sample C036 is highly enriched in quartz, reflecting intense silicification typical of mineralized veins. Sample C046 shows a slightly foliated structure without significant alteration, suggesting a host rock lithology. Finally, C050 is characterized by a quartz-rich matrix with a dark circular structure, indicating heterogeneity favorable for fluid circulation.

2.1. Sample Preparation

The samples were first crushed and then pulverized using a disc/ring mill (DECENT) at the National Geology Laboratory (LNG) of the National Directorate of Geology (DNG) of the Republic of Guinea, in order to obtain a homogeneous powder of approximately 75 µm. Additional grinding was subsequently carried out using a Retsch PM400 planetary mill to further improve homogenization and analytical reproducibility.

After several stages of the reduction process, including mixing and quartering, the sample masses generally ranged between 0.52 g and 0.94 g. To this analytical sample fraction, an internal standard consisting of calcined zinc oxide (ZnO) (5 wt%) was added, followed by complete homogenization of the mixture. The final total mass (sample + standard) ranged from 0.55 g to approximately 1.00 g, thereby ensuring the reliability and reproducibility of the measurements (Table 1).

Table 1 Sample masses and ZnO additions (5 wt.%) for the standard addition calibration method

Sample ID	Depth (m) From–To	Sample weight (g)	Standard weight to add ZnO (g)	Standard weight added (g)	Total weight (g)
C009	161.00 – 161.15	0.5986	0.031505	0.0315	0.6301
C014	97.70 – 97.85	0.5887	0.030984	0.0309	0.6196
C016	146.20 – 146.36	0.7136	0.037558	0.0376	0.7512
C022	84.20 – 84.35	0.5215	0.027447	0.0279	0.5494
C024	115.58 – 115.75	0.7626	0.040137	0.0401	0.8027
C026	142.81 – 142.93	0.5668	0.029832	0.0298	0.5966
C036	104.81 – 105.00	0.8317	0.043774	0.0436	0.8753
C046	93.00 – 93.22	0.9444	0.049705	0.0498	0.9942
C050	122.14 – 122.36	0.7652	0.040274	0.0407	0.8059
C059	129.30 – 129.45	0.8024	0.042232	0.0423	0.8447

Table 1 groups together samples obtained from drill cores of the Kouroussa Project (KGM), collected at depths ranging from approximately 84 m to 161 m.

2.2. X-ray Diffraction (XRD) Analyses

X-ray diffraction (XRD) analyses were performed on powders obtained after mechanical treatment, ensuring a fine and homogeneous grain size distribution. A representative fraction of the samples was prepared in the laboratory, and an internal standard consisting of calcined ZnO (5 wt%) was added to ensure the reliability and reproducibility of the analyses.

The diffractograms were acquired over an angular range of 5° to 80° (2θ) using a Bruker D2 Phaser diffractometer installed at the Geology Laboratory of the Gabriele d'Annunzio University of Chieti-Pescara (UdA), Italy. Analytical conditions included an accelerating voltage of 30 kV, a current of 10 mA, and an acquisition time of 30 minutes per sample.

Mineralogical phase identification was carried out through comparison with crystallographic databases using the DIFFRAC.EVA software, whereas phase quantification was performed by Rietveld refinement using Profex 5 software.

The integration of data derived from field observations, thin-section petrography, and X-ray diffraction analyses enabled a multi-scale approach. This combination made it possible to correlate macroscopic, microscopic, and crystallographic observations, thereby contributing to a better understanding of the mineralogical assemblages and the petro-metallogenic processes associated with the gold mineralization of the Kouroussa permit.

3. Results and Discussion

The X-ray diffraction (XRD) analyses performed on samples C009, C014, C016, C022, C024, C026, C036, C046, C050, and C059 reveal mineralogical assemblages dominated by quartz, feldspars, carbonates, and ferromagnesian minerals, with variable occurrences of sulfides.

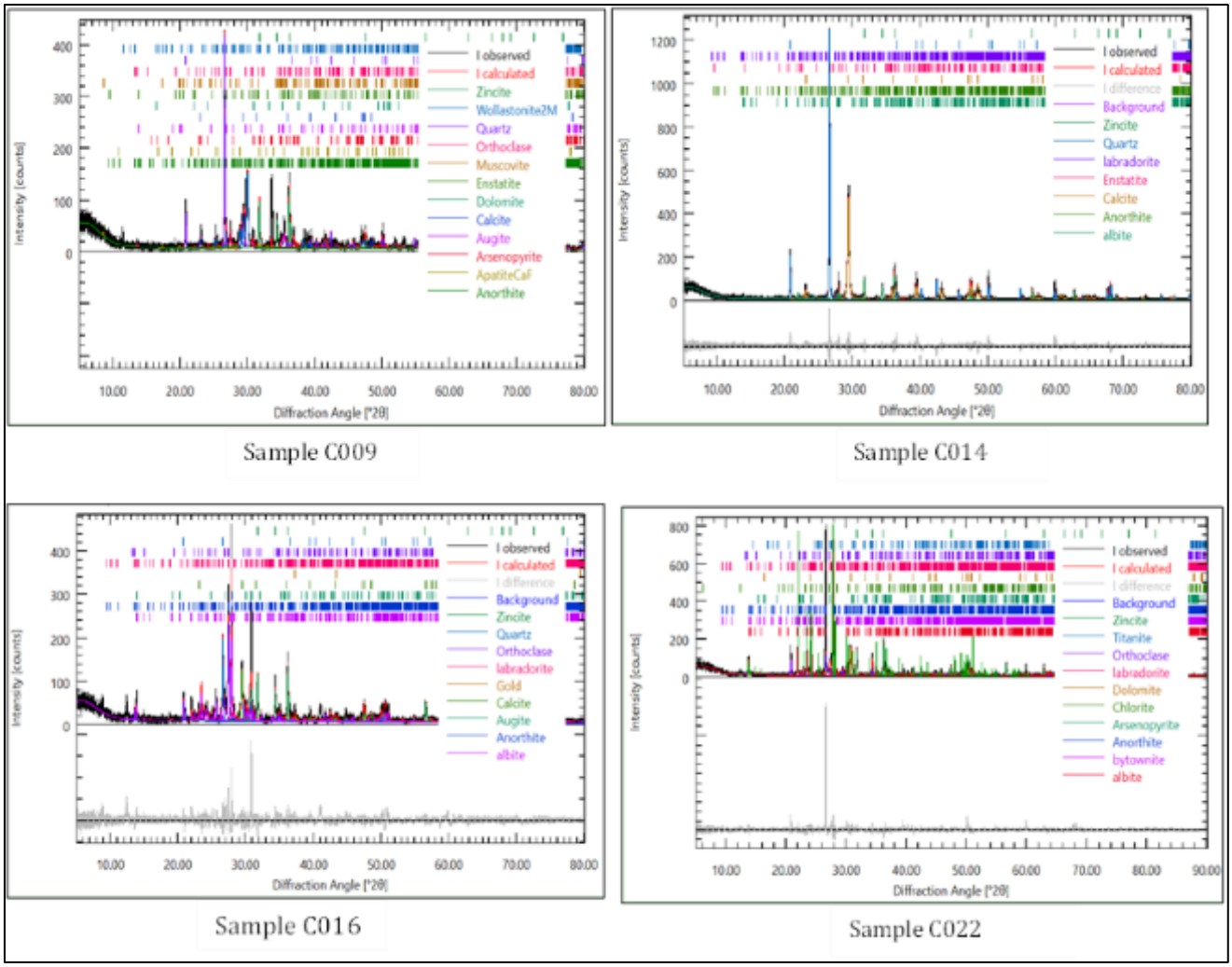
Intensity [counts]
Diffraction Angle [°2θ]
I observed
I calculated
Zincite
Wollastonite2M
Quartz
Orthoclase
Muscovite
Enstatite
Dolomite
Calcite
Augite
Arsenopyrite
ApatiteCaF
Anorthite
Sample C009
I observed
I calculated
I difference
Background
Zincite
Quartz
labradorite
Enstatite
Calcite
Anorthite
albite
Sample C014
I observed
I calculated
I difference
Background
Zincite
Quartz
Orthoclase
labradorite
Gold
Calcite
Augite
Anorthite
albite
Sample C016
I observed
I calculated
I difference
Background
Zincite
Titanite
Orthoclase
labradorite
Dolomite
Chlorite
Arsenopyrite
Anorthite
bytownite
albite
Sample C022

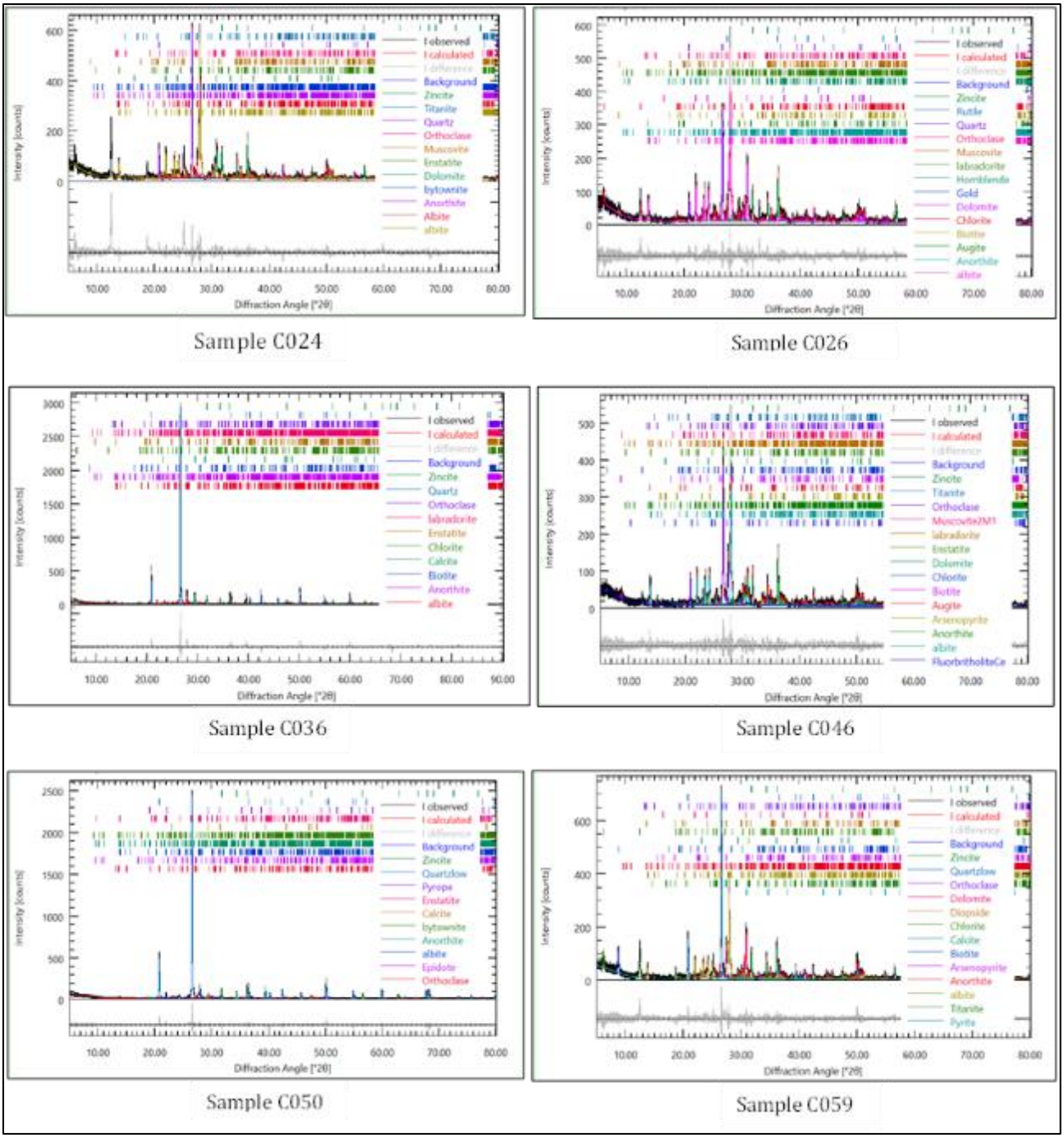

Figure 3 X-ray diffraction (XRD) diffractograms of samples C009, C014, C016, C022, C024, C026, C036, C046, C050, and C059 from the Kouroussa permit, illustrating the main mineral phases identified

Les The obtained diffractograms (Fig. 4) display well-defined characteristic peaks mainly attributable to quartz (Qz), feldspars (Pl, Kfs), carbonates (Cal, Dol, Ank), as well as certain alteration minerals such as chlorite and muscovite. The presence of peaks associated with sulfides (arsenopyrite, pyrite) is observed in some samples, confirming their relationship with gold mineralization [27, 29]. These diffractometric signatures corroborate the petrographic and macroscopic observations described previously.

The quantitative synthesis presented in Table 2 highlights strong variability among the samples, reflecting contrasting formation and alteration conditions.

Samples C036 and C050 are distinguished by a high quartz content (up to 69 wt.%), which is expressed in the diffractograms by dominant high-intensity peaks. This signature indicates intense silicification related to the circulation

of silica-rich hydrothermal fluids. Such silicification is characteristic of orogenic gold systems, where quartz constitutes the principal gangue phase [1,22,23].

In contrast, several samples (C009, C022, C026) display diffractograms dominated by feldspar peaks, reflecting a magmatic heritage consistent with dioritic to granodioritic lithologies. However, the coexistence of these phases with alteration minerals such as chlorite and muscovite, visible on the diffractograms, indicates secondary transformation linked to hydrothermal processes [3,7,24,27].

Furthermore, the presence of ferromagnesian minerals (chlorite, biotite) in several samples, confirmed by XRD signatures, indicates hydrothermal alteration under greenschist facies conditions [9,15]. Carbonates (calcite, ankerite, and dolomite), particularly abundant in sample C014 (~48 wt.%), are expressed by distinct peaks on the diffractograms and reflect hydrothermal carbonation associated with CO_2-rich fluids, a process frequently involved in the formation of gold deposits [3,9,31].

3.1. Metallogenic Significance and Implications for Gold Mineralization

Table 2 highlights the presence of sulfides, particularly arsenopyrite and pyrite, with significant proportions in sample C059 (~11 wt.%).

Table 2 Semi-quantitative mineralogical composition (wt.%) of the samples

Sample	Quartz (wt.%)	Plagioclases (wt.%)	K-feldspar (wt.%)	Carbonates (wt.%)	Ferromagnesian minerals (wt.%)	Sulfides (wt.%)	Accessory minerals (wt.%)
C009	10	69	4	14	10	2	1
C014	27	27	0	48	0	0	11
C016	3	35	24	7	10	<1 (Au)	26
C022	<1	42	18	8	1	1	30
C024	10	36	5	10	0	0	39
C026	8	42	6	11	10	<1 (Au)	23
C036	49	15	3	12	5	0	16
C046	<1	41	7	7	9	2	34
C050	69	14	2	3	1	0	11
C059	21	29	6	13	6	11	14

This table also highlights a strong variability in mineralogical assemblages among the samples, reflecting the combined effects of magmatic, hydrothermal, and metallogenic processes. Two samples are distinguished by marked silicification, namely C036 (49 wt.%) and especially C050 (69 wt.%), indicating intense circulation of silica-rich hydrothermal fluids, whereas C059 (21 wt.%) reflects a more moderate silicification associated with mineralization.

In contrast, several samples (C009, C022, C026, and C046) are dominated by feldspars and plagioclases (up to 73 wt.% combined in C009), reflecting a magmatic heritage related to dioritic to granodioritic host rocks. However, their association with alteration minerals (chlorite, biotite, muscovite) and carbonates indicates subsequent hydrothermal transformation [27]. Carbonates are particularly abundant in C014 (48 wt.%), suggesting hydrothermal carbonation linked to CO_2-rich fluids, which is also evident in C009 and C059. Ferromagnesian minerals (up to 10 wt.% in some samples) indicate greenschist-facies alteration, characteristic of fluid–rock interactions in gold-bearing systems.

Finally, the distribution of sulfides is heterogeneous, with notable enrichment in C059 (11 wt.%), considered the most representative of a mineralized zone, whereas C009 and C046 display moderate contents, and C016 and C026 contain traces of native gold, confirming the gold potential of the system despite overall low concentrations [27,28,29].

These phases are direct indicators of gold mineralization. The arsenopyrite–pyrite association, accompanied by traces of native gold (observed in C016 and C026), confirms that these assemblages belong to an orogenic gold system

[21,29,30,31]. In this type of system, gold is generally trapped within sulfides or precipitated during physicochemical variations of the hydrothermal fluids [5].

The overall analysis of the mineralogical assemblages suggests a multi-stage evolution:

- An initial magmatic phase dominated by feldspars and ferromagnesian minerals,
- A hydrothermal alteration phase characterized by silicification, chloritization, and carbonation,
- A mineralization phase marked by sulfide formation and gold precipitation.

This evolution is consistent with models proposed for gold systems of the West African Craton [27,30].

Finally, the results show that the zones most favorable for gold mineralization are characterized by a combination of silicification, hydrothermal alteration, and the presence of sulfides, thus constituting essential exploration criteria within the Kouroussa permit.

4. Conclusion

The application of X-ray diffraction (XRD) to samples from the Kouroussa permit enabled the precise identification and quantification of major and accessory mineral phases. The quantitative results obtained through Rietveld refinement clearly highlight the strong variability of the mineralogical assemblages.

Sample C050 exhibits the highest quartz content (69 wt.%), reflecting intense silicification characteristic of zones affected by silica-rich hydrothermal fluid circulation. In contrast, sample C014 is dominated by carbonates (48 wt.%), emphasizing the importance of hydrothermal carbonation related to CO_2-rich fluids. Samples C009, C022, and C026 display cumulative feldspar and plagioclase contents of 73, 60, and 48 wt.%, respectively, inherited from dioritic to granodioritic magmatism; however, their association with ferromagnesian alteration minerals (up to 10 wt.% chlorite and biotite) indicates subsequent hydrothermal transformation.

The distribution of sulfides is heterogeneous: sample C059 is distinguished by a content of 11 wt.% arsenopyrite and pyrite associated with 21 wt.% quartz, making it the most representative sample of a mineralized zone. In addition, samples C016 and C026 contain traces of native gold (<1 wt.%), confirming the gold potential of the system. The arsenopyrite–pyrite–native gold association is typical of orogenic gold systems.

Finally, this study demonstrates that XRD, although it presents limitations for amorphous phases or minerals occurring in very low proportions, constitutes a robust and quantitative tool for guiding mineral exploration. The identified criteria — intense silicification (quartz contents >49 wt.%), significant carbonation (>10 wt.% carbonates), substantial sulfide presence (>5 wt.%), and ferromagnesian alteration — are reliable vectors for locating mineralized zones within the Kouroussa permit and, more broadly, within Birimian terranes of West Africa.

Compliance with ethical standards

Acknowledgments

The authors would like to express their sincere gratitude to Kouroussa Gold Mine for granting access to drill cores and geological data used in this study.

The authors also thank the National Geological Laboratory (LNG) of the National Directorate of Geology (DNG) of the Republic of Guinea for their technical support during sample preparation and crushing. Special thanks are addressed to the Geology Laboratory of the Gabriele d'Annunzio University of Chieti-Pescara for providing access to the Bruker D2 Phaser diffractometer and the analytical facilities used for XRD analyses.

The authors also express their appreciation to the EDP-STI of the Félix Houphouët-Boigny National Polytechnic Institute (INP-HB), where I am enrolled and authorized to conduct my PhD research entitled: *"Petrostructural and metallogenic characterization of gold mineralization in the Kouroussa Gold Mine permit, Republic of Guinea."*

Finally, the authors thank all colleagues, laboratory technicians, and field teams who contributed to sample collection, preparation, and analysis, as well as to the scientific discussions that enriched this study.

Disclosure of conflict of interest

The authors declare no conflict of interest, whether financial or non-financial, that could have influenced the results or interpretation of this study.

Statement of ethical approval

The samples analyzed in this study come from geological drill cores collected within the Kouroussa Gold Mine concession, Republic of Guinea, with authorization from the relevant mining and institutional authorities.

References

[1] Daver L, Jébrak M, Beaudoin G, Trumbull R. Three-stage formation of greenstone-hosted orogenic gold deposits in the Val-d'Or mining district, Abitibi, Canada: Evidence from pyrite and tourmaline. Ore Geol Rev. 1 mai 2020;120:103449. doi:10.1016/j.oregeorev.2020.103449

[2] Silyanov S, Sazonov A, Naumov E, Lobastov B, Zvyagina Y, Artemyev D, et al. Mineral Paragenesis, Formation Stages and Trace Elements in Sulfides of the Olympiada Gold Deposit (Yenisei Ridge, Russia). Ore Geol Rev. 1 févr 2022. doi:10.1016/j.oregeorev.2022.104750

[3] Augustin J. Étude des minéralisations aurifères du district de Mana, Burkina Faso. Évolution hydrothermale d'un système aurifère et contraintes tectono-métamorphiques [PhD Thesis]. Université du Québec à Chicoutimi; 2017.

[4] Coulibaly Y, Cathelineau M, Boiron M. Multistage Fluid Evolution and P-T Path at Ity Gold Deposit and Dahapleu Prospect (Western Ivory Coast). Minerals. 28 août 2025. doi:10.3390/min15090918

[5] Dabo M, Aïfa T, Miyouna T, Diallo DA. Gold mineralization paragenesis to tectonic structures in the Birimian of the eastern Dialé-Daléma Supergroup, Kédougou-Kéniéba Inlier, Senegal, West African Craton. Int Geol Rev. 18 mai 2016;58:807-25. doi:10.1080/00206814.2015.1123121

[6] Diallo M, Salvi S, Baratoux L, Béziat D, Vanderhaeghe O, Labou I, et al. Geology of the Tabakoto gold deposit, Kédougou-Kéniéba Inlier, West African Craton, Mali. BSGF - Earth Sci Bull. 22 oct 2024. doi:10.1051/bsgf/2024024

[7] Dzigbodi-Adjimah K. Geology and geochemical patterns of the Birimian gold deposits, Ghana, West Africa. J Geochem Explor. 1 avr 1993;47:305-20. doi:10.1016/0375-6742(93)90073-u

[8] Fofana CM, Olatunji A, Bouaré M, Coulibaly S. A review of the orogenic gold deposits of Southern Mali: structural and metallogenic insights. Int J Sci Res Updat. 30 nov 2025. doi:10.53430/ijsru.2025.10.2.0045

[9] Lawrence DM, Treloar PJ, Rankin AH, Boyce A, Harbidge P. A fluid inclusion and stable isotope study at the Loulo mining district, Mali, West Africa: Implications for multifluid sources in the generation of orogenic gold deposits. Econ Geol. 2013;108(2):229-57.

[10] Ali A, Zhang N, Santos R. Mineral Characterization Using Scanning Electron Microscopy (SEM): A Review of the Fundamentals, Advancements, and Research Directions. Appl Sci. 22 nov 2023. doi:10.20944/preprints202310.2059.v1

[11] Buyse F, Dewaele S, Boone M, Cnudde V. Combining Automated Mineralogy with X-ray Computed Tomography for Internal Characterization of Ore Samples at the Microscopic Scale. Nat Resour Res. 19 janv 2023;32:461-78. doi:10.1007/s11053-023-10161-z

[12] Chen Y, Chen Y, Liu Q, Liu X. Quantifying common major and minor elements in minerals/rocks by economical desktop scanning electron microscopy/silicon drift detector energy-dispersive spectrometer (SEM/SDD-EDS). Solid Earth Sci. 1 janv 2023. doi:10.1016/j.sesci.2022.12.002

[13] Han S, Löhr S, Abbott A, Baldermann A, Farkas J, McMahon W, et al. Earth system science applications of next-generation SEM-EDS automated mineral mapping [Internet]. Vol. 10. 23 nov 2022;10. doi:10.3389/feart.2022.956912

[14] Liu P, Wang Z, Zhang Z. A New Quantitative Approach for Element-Mineral Determination Based on "EDS (Energy Dispersive Spectroscopy) Method". Geofluids. 27 août 2021. doi:10.1155/2021/4023704

[15] Lynch G, Mengel F. Metamorphism of arsenopyrite-pyrite-sphalerite-pyrrhotite lenses, western Cape Breton Island, Nova Scotia. Can Mineral. 1995;33(1):105-14.

[16] Schulz B, Sandmann D, Gilbricht S. SEM-Based Automated Mineralogy and Its Application in Geo- and Material Sciences. Minerals. 11 nov 2020;10:1004. doi:10.3390/min10111004

[17] Bunaciu A, Udriştioiu EG, Aboul-Enein H. X-Ray Diffraction: Instrumentation and Applications. Crit Rev Anal Chem. 1 avr 2015;45:289-99. doi:10.1080/10408347.2014.949616

[18] Singh GVPB, Subramaniam K. Quantitative XRD study of amorphous phase in alkali activated low calcium siliceous fly ash. Constr Build Mater. 15 oct 2016;124:139-47. doi:10.1016/j.conbuildmat.2016.07.081

[19] Zhao P, Liu X, Torre Á, Lu L, Sobolev K. Assessment of the quantitative accuracy of Rietveld/XRD analysis of crystalline and amorphous phases in fly ash. Anal Methods. 20 avr 2017;9:2415-24. doi:10.1039/c7ay00337d

[20] Djagre L, Koffi BG, Camara M, Ouattara G, Agbossoumondé Y. The metasedimentary-hosted Nyangoubé gold prospect, northwest Côte d'Ivoire: Geochemical and mineralogical characterization of associated hydrothermal alteration. Heliyon. 1 sept 2023;9. doi:10.1016/j.heliyon.2023.e20227

[21] Mignot E, Siebenaller L, Béziat D, André-Mayer A, Reisberg L, Salvi S, et al. The Paleoproterozoic Copper-Gold Deposits of the Gaoua District, Burkina Faso: Superposition of Orogenic Gold on a Porphyry Copper Occurrence? Econ Geol. 1 janv 2017;112:99-122. doi:10.2113/econgeo.112.1.99

[22] Chen B, Zuo YJ, Zheng L, Liu J, Sun W, Lin J, et al. Relationship between silicification and gold mineralization and evolution of hydrothermal systems in Nibao Carlin-type gold deposits, SW China: Insights from rock geochemistry and trace elements of quartz and pyrite. Ore Geol Rev. 1 déc 2024. doi:10.1016/j.oregeorev.2024.106394

[23] Wu Y, Li JW, Evans K, Koenig A, Li Z, O'Brien H, et al. Ore-Forming Processes of the Daqiao Epizonal Orogenic Gold Deposit, West Qinling Orogen, China: Constraints from Textures, Trace Elements, and Sulfur Isotopes of Pyrite and Marcasite, and Raman Spectroscopy of Carbonaceous Material. Econ Geol. 1 août 2018. doi:10.5382/econgeo.2018.4583

[24] Ballouard C, Elburg M, Tappe S, Reinke C, Ueckermann H, Doggart S. Magmatic-hydrothermal evolution of rare metal pegmatites from the Mesoproterozoic Orange River pegmatite belt (Namaqualand, South Africa). Ore Geol Rev. 26 nov 2019;116:103252. doi:10.1016/j.oregeorev.2019.103252

[25] Feng J, Tang L, Santosh M, Zhang S, Sheng Y, Hu XK, et al. Genesis of hydrothermal gold mineralization in the Qianhe deposit, central China: Constraints from in situ sulphur isotope and trace elements of pyrite. Geol J. 2 déc 2020;56:3241-56. doi:10.1002/gj.4099

[26] Scaillet B. Mémoire présenté en vue de l'obtention de l'Habilitation à Diriger des Recherches [PhD Thesis] [Internet]. Université d'Orléans; 2006 [cité 22 avr 2026]. Disponible sur: https://theses.hal.science/tel-00077395/

[27] Widiatmoko F, Sari A, Ramadhanty J, Putri R. Study of Hydrothermal Alteration and Mineralization in the Lahbako Field, Jember Regency, East Java Province. In: Vol. 2117. 2021. Disponible sur: https://consensus.app/papers/study-of-hydrothermal-alteration-and-mineralization-in-widiatmoko-sari/f0297aa3ffef531586a0d3a9af4f6816/ doi:10.1088/1742-6596/2117/1/012004

[28] Beavogui M. Structural Controls of Gold Mineralisation in Seguelen Pit of Siguiri Gold Mine, Guinea [PhD Thesis] [Internet]. Rhodes University; 2014 [cité 12 nov 2024]. Disponible sur: https://core.ac.uk/download/pdf/145046661.pdf

[29] Lebrun EO. 4D evolution of the orogenic gold district of Siguiri, Guinea (West Africa). 2016.

[30] Le Mignot É. Les gisements d'or comme témoins de l'histoire géologique du craton oues-africain : apports de la datation [These de doctorat] [Internet]. Université de Lorraine; 2014 [cité 31 mai 2022]. Disponible sur: https://www.theses.fr/2014LORR0269

[31] Yollande Traoré. Etude métallogénique du district aurifère de Syama (Mali) : analyse comparative de gisements situés sur une même structure lithosphérique éburnéenne [These de doctorat]. [Internet]. Minéralogie. Université Paul Sabatier - Toulouse III, 2017. Français. ⟨NNT : 2017TOU30087⟩. ⟨tel-01900948⟩